Quantum Correlations in Optical Angle Orbital Angular Momentum Variables

Jonathan Leach, *et al.*

Science **329**, 662 (2010);
DOI: 10.1126/science.1190523

surface states (*18*). This optimally doped sample thus fully realizes the insulating massive Dirac fermion state and provides a model system for studying striking topological phenomena (*5*, *20*–*22*).

To maintain this insulating massive Dirac fermion state at higher temperatures requires a further increase of the Dirac gap (while keeping E_F inside it). However, because of the hole-doping effect of Mn dopants, one cannot simply increase the Mn concentration in $(Bi_{1-\delta}Mn_\delta)_2Se_3$ to acquire a larger Dirac gap, as the system will become p-type before the gap magnitude increases appreciably (*19*). However, we found that it was possible to introduce many Fe dopants into Bi_2Se_3 to increase the gap size without substantially altering the E_F position relative to the undoped Bi_2Se_3; if we can then move E_F into the gap by introducing additional p-type dopants, we can achieve a larger gap while preserving the insulating nature of the state.

Figure 4 demonstrates the full range of E_F tuning by introducing such p-type doping, with three doping regions and the topological transport point (where E_F coincides with the Dirac point) shown in Fig. 4A. By either surface doping [Fig. 4B and (*19*)] or bulk doping (Fig. 4, C to F), we were able to tune the E_F to any of the regions defined in Fig. 4A. The ability to convert the original n-type sample to p-type by surface doping (Fig. 4B, region III) is critical for applications requiring both types of carriers or p-n junctions. On the other hand, full-range bulk doping (Fig. 4, C to F) has advantages over surface doping in bulk applications.

References and Notes

1. B. A. Bernevig, T. L. Hughes, S.-C. Zhang, *Science* **314**, 1757 (2006).
2. M. König *et al.*, *Science* **318**, 766 (2007); published online 20 September 2007 (10.1126/science.1148047).
3. X. L. Qi, S. C. Zhang, *Phys. Today* **63**, 33 (2010).
4. L. Fu, C. L. Kane, E. J. Mele, *Phys. Rev. Lett.* **98**, 106803 (2007).
5. X. L. Qi, T. L. Hughes, S. C. Zhang, *Phys. Rev. B* **78**, 195424 (2008).
6. A. P. Schnyder, S. Ryu, A. Furusaki, A. W. Ludwig, *Phys. Rev. B* **78**, 195125 (2008).
7. L. Fu, C. L. Kane, *Phys. Rev. Lett.* **102**, 216403 (2009).
8. A. R. Akhmerov, J. Nilsson, C. W. J. Beenakker, *Phys. Rev. Lett.* **102**, 216404 (2009).
9. J. E. Moore, L. Balents, *Phys. Rev. B* **75**, 121306(R) (2007).
10. R. Roy, *Phys. Rev. B* **79**, 195321 (2009).
11. B. Seradjeh, J. E. Moore, M. Franz, *Phys. Rev. Lett.* **103**, 066402 (2009).
12. H. Zhang *et al.*, *Nat. Phys.* **5**, 438 (2009).
13. Y. Xia *et al.*, *Nat. Phys.* **5**, 398 (2009).
14. Y. L. Chen *et al.*, *Science* **325**, 178 (2009); published online 11 June 2009 (10.1126/science.1173034).
15. J. Choi *et al.*, *Phys. Status Solidi B* **241**, 1541 (2004).
16. Y. S. Hor *et al.*, *Phys. Rev. B* **81**, 195203 (2010).
17. R. Yu *et al.*, *Science* **329**, 61 (2010); published online 3 June 2010 (10.1126/science.1187485).
18. Q. Liu, C. X. Liu, C. K. Xu, X. L. Qi, S. C. Zhang, *Phys. Rev. Lett.* **102**, 156603 (2009).
19. See supporting material on *Science* Online.
20. X.-L. Qi, R. Li, J. Zang, S.-C. Zhang, *Science* **323**, 1184 (2009); published online 29 January 2009 (10.1126/science.1167747).
21. J. Zang, N. Nagaosa, *Phys. Rev. B* **81**, 245125 (2010).
22. F. Wilczek, *Nature* **458**, 129 (2009).
23. L. Fu, *Phys. Rev. Lett.* **103**, 266801 (2009).
24. X. Zhou, C. Fang, W. F. Tsai, J. P. Hu, *Phys. Rev. B* **80**, 245317 (2009).
25. W. C. Lee, C. Wu, D. P. Arovas, S. C. Zhang, *Phys. Rev. B* **80**, 245439 (2009).
26. Z. Alpichshev *et al.*, *Phys. Rev. Lett.* **104**, 016401 (2010).
27. T. Zhang *et al.*, http://arxiv.org/abs/0908.4136 (2009).

28. Supported by the Department of Energy, Office of Basic Energy Science, under contract DE-AC02-76SF00515.

Supporting Online Material

www.sciencemag.org/cgi/content/full/329/5992/659/DC1
Materials and Methods
SOM Text
Figs. S1 to S6
Movies S1 to S3
References

22 March 2010; accepted 16 June 2010
10.1126/science.1189924

Quantum Correlations in Optical Angle–Orbital Angular Momentum Variables

Jonathan Leach,[1] Barry Jack,[1] Jacqui Romero,[1] Anand K. Jha,[2] Alison M. Yao,[3] Sonja Franke-Arnold,[1] David G. Ireland,[1] Robert W. Boyd,[2] Stephen M. Barnett,[3] Miles J. Padgett[1]*

Entanglement of the properties of two separated particles constitutes a fundamental signature of quantum mechanics and is a key resource for quantum information science. We demonstrate strong Einstein, Podolsky, and Rosen correlations between the angular position and orbital angular momentum of two photons created by the nonlinear optical process of spontaneous parametric down-conversion. The discrete nature of orbital angular momentum and the continuous but periodic nature of angular position give rise to a special sort of entanglement between these two variables. The resulting correlations are found to be an order of magnitude stronger than those allowed by the uncertainty principle for independent (nonentangled) particles. Our results suggest that angular position and orbital angular momentum may find important applications in quantum information science.

In 1935, Einstein, Podolsky, and Rosen (EPR) proposed a Gedanken experiment that was intended to show that quantum mechanics is incomplete (*1*). Their proposal supposes the existence of two spatially separated particles that are perfectly correlated in both position and momentum. Measurement of the position (or alternatively the momentum) of one particle would then determine instantaneously the position (or momentum) of the second particle. The ability to infer either the position or the momentum of the second particle from a distant measurement on the first seems to imply that both of these quantities must have been predetermined. However, quantum theory (and specifically the uncertainty principle) does not allow the simultaneous, exact knowledge of two noncommuting observables, such as position and momentum, as seems to be required for the second particle. A demonstration of EPR correlations establishes either that quantum mechanics is incomplete, in that systems possess additional hidden variables, or that quantum mechanics is nonlocal, in that measurement of the position or momentum of either particle results in an instantaneous uncertainty of the momentum or position, respectively, of both (*2*).

In 1964, Bell deduced an inequality that distinguishes the predictions of quantum theory from those of any local hidden variable theory (*3*, *4*). Since that time, many experiments have been performed that have decided strongly in favor of quantum theory (*5*, *6*). These Bell-type tests apply only to discrete state-spaces, originally of two dimensions or, more recently, to three or higher dimensions (*7*–*9*). In contrast, EPR correlations provide a demonstration of entanglement both for discrete and continuous variables, such as energy and time (*10*), position and linear momentum (*11*), spatial modes (*12*, *13*), and images (*14*).

In addition to linear momentum, light may also carry angular momentum. The spin angular momentum is manifest as the polarization of light and is described completely within a two-dimensional Hilbert space. However, light beams can also carry a measurable orbital angular momentum that results from their helical phase structure. This phase structure can be described by $\exp(i\ell\phi)$(*15*, *16*), where ϕ is the azimuthal angle and ℓ can take any integer value, corresponding to an orbital angular momentum in the direction of propagation of $L_z = \ell\hbar$ per photon, where $\hbar$ is Planck's constant h divided by 2π. For restricted subspaces of two or three dimensions, the orbital angular momentum variable has previously been shown to be an entangled property of down-converted photon pairs (*17*, *18*) and to violate a

[1]Department of Physics and Astronomy, Scottish Universities Physics Alliance (SUPA), University of Glasgow, Glasgow, G12 8QQ, UK. [2]Institute of Optics, University of Rochester, Rochester, NY 14627, USA. [3]Department of Physics, SUPA, University of Strathclyde, Glasgow, G4 0NG, UK.

*To whom correspondence should be addressed. E-mail: m.padgett@physics.gla.ac.uk

Bell-type inequality (*19*, *20*). However, these present measurements are different in that they are performed in conjunction with the measurement of angular position, the variable conjugate to angular momentum, and hence demonstrate the existence of EPR correlations.

The probability distributions for linear momentum and position are simply Fourier transforms of each other, and the relationship between the standard deviations of their distributions is expressed in the familiar Heisenberg uncertainty relation $\Delta x \Delta p \geq \hbar/2$. In contrast, angle is 2π periodic, and so the Fourier relation between angular position and angular momentum has a different form (*21*, *22*). The periodic, and therefore bounded, angular variable is expressed as a discrete and unbounded Fourier series of angular momenta. Indeed, it is this angular periodicity that gives the quantized—that is, discrete—nature of angular momentum.

We established experimentally that entanglement, as manifest by EPR correlations, exists for angular variables (*23*). Our apparatus is based on parametric down-conversion, in which a quasi-continuous-wave, mode-locked ultraviolet pump beam at 355 nm is incident on a 3-mm length of nonlinear crystal [β-barium borate (BBO)] (Fig. 1) (*24*).

Key to our approach is that just as the spatial light modulator (SLM) can be programmed to transform the fundamental near-Gaussian mode emitted from a fiber into any complex spatial mode of choice, if operated in reverse the same hologram can efficiently couple the same complicated mode distribution back into a fiber. In this configuration, the SLM acts as a mode filter, allowing the transverse spatial state of the down-converted photons to be inferred. Although SLMs have previously been used to measure the orbital angular momentum of down-converted photons (*25*, *26*), we used a spatial variation in the blazing function (*27*) to also measure the angular position of the down-converted photons. The advantage of SLMs over static holographic components, or other phase filters, is that they can be electronically programmed to switch among different arbitrary measurement states.

To measure the orbital angular momentum state ℓ of the detected photon, we used the typical forked diffraction grating that has been widely implemented for beam generation (*28*) and single-photon measurement (*17*, *25*). The SLM is programmed with a spatial phase variation $\Phi(x, y)$, centered at $x = 0$, $y = 0$, given by

$$\Phi(x,y) = |\ell(\arctan\, x/y) + 2\pi\Lambda x|_{\mathrm{mod}2\pi} \quad (1)$$

where Λ is the period of the linear grating, to separate the first-order diffracted beam. Changing the order ℓ of the fork dislocation in the center of the hologram allows sequential measurement of an arbitrarily wide range of orbital angular momentum states. Alternatively, to measure the angular position we defined a Gaussian-profile, angular-sector transmission aperture that can be varied both in its width θ and orientation ϕ. A narrower aperture gives an inherently more precise measurement of angular position but with a commensurately lower signal. The SLM is programmed with a spatial phase variation $\Phi(x, y)$ given by

$$\Phi(x,y) = |2\pi\Lambda x|_{\mathrm{mod}2\pi} \times \mathrm{sinc}^2\left(\pi\left(1 - \left(\exp\frac{-(\arctan(x/y) - \phi)^2}{\theta^2}\right)\right)\right) \quad (2)$$

where the sinc term effectively sets the depth of the blazing to produce the desired intensity mask (*27*). The angle $(\arctan(x/y) - \phi)$ is taken to be equal to the offset from the center of the aperture of width θ (we circumvented the numerical ambiguity in the vicinity of the angular origin). Although the Gaussian profile does correspond strictly to the minimum uncertainty state (*29*), the precise profile and minimum width of the sector apertures are not central to our argument nor to the results.

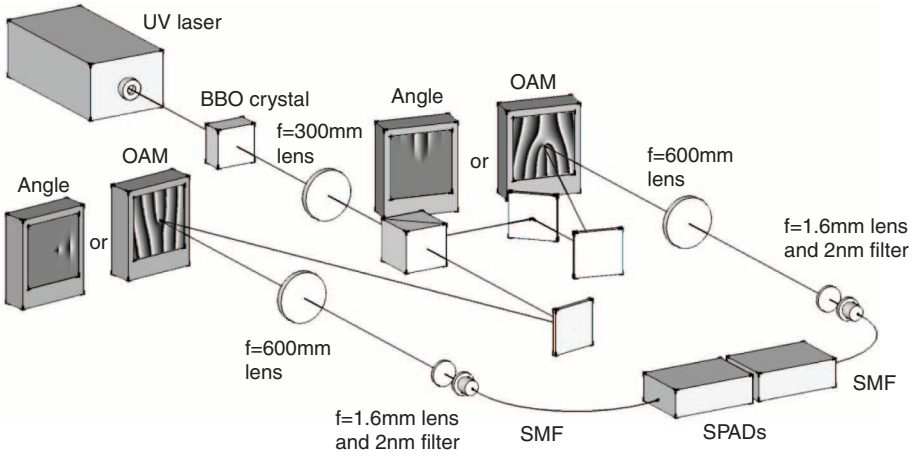

Fig. 1. Schematic of the experiment. The nonlinear BBO crystal is imaged onto two SLMs, one in the signal arm and one in the idler arm. The SLMs are then imaged onto single-mode fibers, coupling the light to SPAD detectors (single-photon avalanche photo-diodes) from which the signals are routed to coincidence-counting electronics. The SLMs can be used to measure either the angular correlations or the orbital angular momentum (OAM) correlations of the entangled fields.

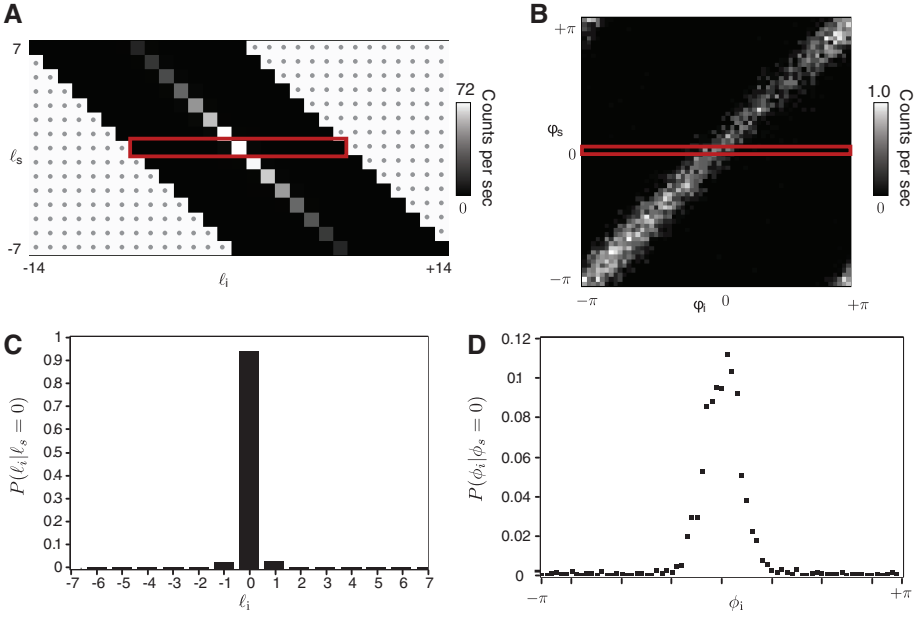

Fig. 2. Experimental results. (**A**) The coincidence count rate as a function of the measured orbital angular momentum in the signal and idler arms (corresponding to ≈20 hours of data collection). (**B**) The coincidence count rate as a function of the orientation of the sector apertures in the signal and idler arms (corresponding to ≈200 hours of data). (**C**) Conditional probability distribution of the orbital angular momentum of the idler photon for the case $\ell_s = 0$, corresponding to the row highlighted in red in (A). (**D**) Similarly, the conditional probability of the angular position ϕ_i is shown for $\phi_s = 0$.

When either the signal or idler beam is viewed independently, the lack of constraint on its phase structure implies that a spatially coherent pump beam creates spatially incoherent down-converted light (*30*), with a speckle size dictated by the phase-matching bandwidth of the crystal. The size of this speckle with respect to the pump beam sets the modal spatial bandwidth of the incoherent output. For a plane-wave or Gaussian pump beam, conservation of orbital angular momentum between the signal and idler photons results in a high coincidence count rate whenever $\ell_s + \ell_i = 0$. However, the strength is modulated by the envelope of the generated modal bandwidth (*31*) and further modified by the relative detection efficiency of the different states. Similarly, for measurements made in an image plane of the crystal the coincidence count rate for angular measurements is highest whenever $\phi_s - \phi_i = 0$.

In practice, perfect correlations in both orbital angular momentum and angular position of the down-converted pairs are unobtainable. In order to demonstrate EPR correlations, we used the more experimentally useful criterion that is based on measuring the conditional probability of finding a particular outcome in one system given a measurement in the other (*32*). Angular momentum is discrete, and angular position is periodic. However, for narrow apertures the Fourier relationship between their variances is the same as for the unbounded continuous case (*22*), and we can write the EPR-Reid criterion as a violation of the inequality

$$(\Delta_{\text{inf}}\ell_s)^2(\Delta_{\text{inf}}\phi_s)^2 \geq 1/4 \qquad (3)$$

The measured angular momentum and angle correlations are shown in Fig. 2, A and B. In both cases, the actual value of the angular momentum or position in the signal and idler beams is not important; rather, it is the difference between measurements in the signal and idler beams that determines the widths of the probability distributions. Also, the precise form of the angular aperture is not important; rather, it is the width of the measured correlation made with respect to the central position of the two apertures.

For the orbital angular momentum states, we measured all combinations of ℓ_s from –7 to +7 and ℓ_i from $\ell_s - 7$ to $\ell_s + 7$, corresponding to the approximate spiral bandwidth of our system. For the angular states, we used an angular aperture width of $\theta = \pi/15$ and measured all combinations of ϕ_s and ϕ_i in 60 equally spaced angular bins. The measured correlations shown in Fig. 2, A and B, are maximal whenever $\ell s + \ell_i = 0$ or $\phi_s - \phi_i = 0$, respectively. Shown in Fig. 2, C and D, are single sections through this data, illustrating the strength of the angular momentum and angle correlations.

As with all experimental data, small amounts of random noise can adversely affect the statistical estimate of the variance of a distribution. We minimized this noise by running the experiment at a low flux (≈20,000 photon pairs s^{-1}), which minimizes the number of accidental coincidence counts arising from classical correlations.

Without any background subtraction, we obtained $(\Delta_{\text{inf}}\ell_s)^2 = 0.348 \pm 0.022$ and $(\Delta_{\text{inf}}\phi_s)^2 = 0.456 \pm 0.012$, giving a variance product of 0.159 ± 0.011, which is approximately half of the lower bound of 0.25 required by the EPR argument.

We can also calculate the strength of the correlations when we subtract our best estimate of the background counts. For each measured number of coincidence counts N, we inferred the number of true coincidences C and accidental coincidences B so that $B + C = N$. Using the expected number of accidentals, calculated from $S_sS_i\Delta t$, the probability of a count being an accidental coincidence is taken to be $r = \text{Min}[1, S_sS_i\Delta t/N]$, so that the maximum probability is unity. The expectation value of B is then $\langle B\rangle = Nr$. This enables a subtraction of accidental counts but ensures that we obtain nonnegative values for the calculation of probability or entropy.

Subtracting this calculated background to remove accidental coincidences, we obtained $(\Delta_{\text{inf}}\ell_s)^2 = 0.171 \pm 0.018$ and $(\Delta_{\text{inf}}\phi_s)^2 = 0.140 \pm 0.007$, giving a variance product of 0.024 ± 0.004, approximately one tenth of the lower bound required by the EPR argument, hence showing a strong demonstration of the effect.

We also adopted an alternative EPR criterion that is based on entropy rather than variance (*33*–*37*). This approach has a number of advantages. First, the entropic uncertainty relation does not require the calculation of a variance, and the calculation of entropy does not require us to deal with the complications associated with the cyclic nature of the angular variable (*38*, *39*). Secondly, the inequality is state-independent (*35*, *36*), which makes it possible to make a quantitative comparison of our EPR experiment with those reported for different physical systems. Finally, the entropic approach relates the strength of the correlations to the quantum information content of the system (*37*). The entropic uncertainty relation for angular position and angular momentum is (*35*, *36*)

$$H(\ell) + H(\phi) \geq \log_2(2\pi) \qquad (4)$$

where $H(\ell) = -\sum_{\ell} P(\ell)\log_2 P(\ell)$ and $H(\phi) = -\int_{-\pi}^{\pi} d\phi P(\phi)\log_2 P(\phi)$ are the Shannon entropies for the discrete angular momentum variable ℓ and the continuous angle variable ϕ, respectively. We measured the angle in discrete segments, with N segments filling the 2π interval. Direct comparison with our data, therefore, requires us to write our angle entropy in terms of the measured probabilities for these discrete segments ϕ^m as (*36*)

$$H(\phi) = -\sum_m P(\phi_s^m)\log_2 P(\phi^m) - \log_2\left(\frac{N}{2\pi}\right) \qquad (5)$$

A demonstration of EPR correlations corresponds to a violation of the entropic uncertainty relation for the inferred values, which is a violation of the inequality

$$H_{\text{inf}}(\ell_s) + H_{\text{inf}}(\phi_s) = -\sum_{\ell_s,\ell_i} P(\ell_i)P(\ell_s|\ell_i)\log_2 P(\ell_s|\ell_i) - \int_{-\pi}^{\pi} d\phi_i \int_{-\pi}^{\pi} d\phi_s P(\phi_i)P(\phi_s|\phi_i)\log_2 \times P(\phi_s|\phi_i) \geq \log_2(2\pi) \qquad (6)$$

Using the data presented in Fig. 2, A and B, we obtained values of 1.548 ± 0.017 and 0.887 ± 0.018 for $H_{\text{inf}}(\ell_s) + H_{\text{inf}}(\phi_s)$, without and with background subtraction, respectively. Both of these values are significantly below the EPR limit of 2.651.

The results confirm that the EPR conclusion, namely that quantum mechanics is incomplete or nonlocal, applies not only to position and momentum but also to angular position and angular momentum. Unlike demonstrations of Bell-type inequalities, which are restricted to discrete state spaces, EPR correlations simultaneously span an extended range of orbital angular momentum states and the continuous state space of angular position. The demonstration of angular EPR correlations establishes that angular position and angular momentum are suitable variables for applications in quantum information processing, notably in protocols for quantum key distribution (*40*).

References and Notes

1. A. Einstein, B. Podolsky, N. Rosen, *Phys. Rev.* **47**, 777 (1935).
2. M. D. Reid *et al.*, *Rev. Mod. Phys.* **81**, 1727 (2009).
3. J. S. Bell, *Physics* **1**, 195 (1964).
4. J. S. Bell, *Speakable and Unspeakable in Quantum Mechanics* (Cambridge Univ. Press, New York, 1987).
5. S. J. Freedman, J. F. Clauser, *Phys. Rev. Lett.* **28**, 938 (1972).
6. A. Aspect, P. Grangier, G. Roger, *Phys. Rev. Lett.* **49**, 91 (1982).
7. A. Vaziri, G. Weihs, A. Zeilinger, *Phys. Rev. Lett.* **89**, 240401 (2002).
8. N. K. Langford *et al.*, *Phys. Rev. Lett.* **93**, 053601 (2004).
9. D. Collins, N. Gisin, N. Linden, S. Massar, S. Popescu, *Phys. Rev. Lett.* **88**, 040404 (2002).
10. P. G. Kwiat, A. M. Steinberg, R. Y. Chiao, *Phys. Rev. A* **47**, R2472 (1993).
11. J. C. Howell, R. S. Bennink, S. J. Bentley, R. W. Boyd, *Phys. Rev. Lett.* **92**, 210403 (2004).
12. K. Wagner *et al.*, *Science* **321**, 541 (2008).
13. M. Lassen, G. Leuchs, U. L. Andersen, *Phys. Rev. Lett.* **102**, 163602 (2009).
14. V. Boyer, A. M. Marino, R. C. Pooser, P. D. Lett, *Science* **321**, 544 (2008).
15. L. Allen, M. W. Beijersbergen, R. J. Spreeuw, J. P. Woerdman, *Phys. Rev. A* **45**, 8185 (1992).
16. S. Franke-Arnold, L. Allen, M. J. Padgett, *Laser Photon. Rev.* **2**, 299 (2008).
17. A. Mair, A. Vaziri, G. Weihs, A. Zeilinger, *Nature* **412**, 313 (2001).
18. J. B. Pors *et al.*, *Phys. Rev. Lett.* **101**, 120502 (2008).
19. A. Vaziri, G. Weihs, A. Zeilinger, *Phys. Rev. Lett.* **89**, 240401 (2002).
20. J. Leach *et al.*, *Opt. Express* **17**, 8287 (2009).

21. S. M. Barnett, D. T. Pegg, *Phys. Rev. A* **42**, 6713 (1990).
22. S. Franke-Arnold *et al*., *N. J. Phys.* **6**, 103 (2004).
23. J. Götte, S. M. Barnett, S. Franke-Arnold, *J. Mod. Opt.* **53**, 627 (2006).
24. Materials and methods are available as supporting material on *Science* Online.
25. E. Yao, S. Franke-Arnold, J. Courtial, M. J. Padgett, S. M. Barnett, *Opt. Express* **14**, 13089 (2006).
26. M. Stotz, S. Gröblacher, T. Jennewein, A. Zeilinger, *Appl. Phys. Lett.* **90**, 261114 (2007).
27. J. Leach, M. Dennis, J. Courtial, M. Padgett, *N. J. Phys.* **7**, 55 (2005).
28. V. Bazhenov, M. Vasnetsov, M. Soskin, *JETP Lett.* **52**, 429 (1990).
29. D. T. Pegg, S. M. Barnett, R. Zambrini, S. Franke-Arnold, M. Padgett, *N. J. Phys.* **7**, 62 (2005).
30. J. Arlt, K. Dholakia, L. Allen, M. Padgett, *Phys. Rev. A* **59**, 3950 (1999).
31. J. Torres, A. Alexandrescu, L. Torner, *Phys. Rev. A* **68**, 050301 (2003).
32. M. D. Reid, *Phys. Rev. A* **40**, 913 (1989).
33. S. P. Walborn, B. G. Taketani, A. Salles, F. Toscano, R. L. de Matos Filho, *Phys. Rev. Lett.* **103**, 160505 (2009).
34. S. P. Walborn, A. Salles, R. M. Gomes, F. Toscano, P. H. Souto Ribeiro, "An Entropic Einstein-Podolsky-Rosen Criterion" available at arXiv:0907.4263v1 (2009).
35. I. Bialynicki-Birula, J. Mycielski, *Commun. Math. Phys.* **44**, 129 (1975).
36. A. Rojas-Gonzales, J. A. Vaccaro, S. M. Barnett, *Phys. Lett. A* **205**, 247 (1995).
37. S. M. Barnett, S. J. D. Phoenix, *Phys. Rev. A* **40**, 2404 (1989).
38. S. M. Barnett, D. T. Pegg, *J. Mod. Opt.* **36**, 7 (1989).
39. G. M. Forbes, M. A. Alonso, A. E. Siegman, *J. Phys. Math. Gen.* **36**, 1 (2003).
40. F. Grosshans, N. J. Cerf, *Phys. Rev. Lett.* **92**, 047905 (2004).

41. This work is supported by the UK Engineering and Physical Sciences Research Council. S.F.A. is a Research Councils UK Research Fellow. S.M.B. and M.J.P. thank the Royal Society and the Wolfson Foundation. We thank J. Götte and D. Oi for useful discussions. We acknowledge the financial support of the Future and Emerging Technologies (FET) program within the Seventh Framework Programme for Research of the European Commission, under the FET Open grant agreement HIDEAS number FP7-ICT-221906. We would like to thank Hamamatsu for their support of this work. A.K.J. and R.W.B. were supported by a U.S. Department of Defense Multidisciplinary University Research Initiative award. The experiment was devised by J.L., M.J.P., and A.K.J. and performed by J.L., B.J., and J.R. D.I. designed the coincidence-counting electronics. S.M.B. and A.M.Y. formulated the inequalities. The results were interpreted and the manuscript drafted by M.J.P., S.M.B., A.M.Y., J.L., R.W.B., and S.F.A., with further inputs from all authors.

Supporting Online Material

www.sciencemag.org/cgi/content/full/329/5992/662/DC1
Materials and Methods

6 April 2010; accepted 22 June 2010
10.1126/science.1190523

MESSENGER Observations of Extreme Loading and Unloading of Mercury's Magnetic Tail

James A. Slavin,[1]* Brian J. Anderson,[2] Daniel N. Baker,[3,4] Mehdi Benna,[5,6] Scott A. Boardsen,[1,6] George Gloeckler,[7,8] Robert E. Gold,[2] George C. Ho,[2] Haje Korth,[2] Stamatios M. Krimigis,[2,9] Ralph L. McNutt Jr.,[2] Larry R. Nittler,[10] Jim M. Raines,[7] Menelaos Sarantos,[1,6] David Schriver,[11] Sean C. Solomon,[10] Richard D. Starr,[12] Pavel M. Trávníček,[11,13] Thomas H. Zurbuchen[7]

During MESSENGER's third flyby of Mercury, the magnetic field in the planet's magnetic tail increased by factors of 2 to 3.5 over intervals of 2 to 3 minutes. Magnetospheric substorms at Earth are powered by similar tail loading, but the amplitude is lower by a factor of ~10 and typical durations are ~1 hour. The extreme tail loading observed at Mercury implies that the relative intensity of substorms must be much larger than at Earth. The correspondence between the duration of tail field enhancements and the characteristic time for the Dungey cycle, which describes plasma circulation through Mercury's magnetosphere, suggests that such circulation determines the substorm time scale. A key aspect of tail unloading during terrestrial substorms is the acceleration of energetic charged particles, but no acceleration signatures were seen during the MESSENGER flyby.

Magnetospheric substorms are space weather disturbances powered by the rapid release of magnetic energy stored in the lobes of planetary magnetic tails (*1*). The loading and unloading of Earth's tail occurs on time scales of ~1 hour and is closely correlated with a southward component of the interplanetary magnetic field (IMF) (i.e., opposite to the planetary magnetic field at the nose of the magnetosphere), a geometry that transports magnetic flux into the tail via magnetic reconnection between the IMF and the dayside geomagnetic field (*2*). During a substorm, the accumulated magnetic energy is unloaded through reconnection of the oppositely directed magnetic fields in the tail lobes, resulting in the ejection of plasmoids, high-speed sunward and antisunward jetting of hot plasma, acceleration and injection of charged particles into the inner magnetosphere, and field-aligned currents flowing between the tail and the high-latitude atmosphere where aurorae are produced (*3*). Here, we report observations by the MErcury Surface, Space ENvironment, GEochemistry, and Ranging (MESSENGER) spacecraft of substorm-like magnetic tail-loading events at Mercury.

This circulation of plasma, magnetic flux, and energy from the dayside X-line at the terrestrial magnetopause to the nightside X-line in the cross-tail current layer and, later, back to the dayside magnetosphere constitutes the Dungey cycle (*4*), whose energy is drawn from the solar wind. The large magnetic field component normal to the magnetopause measured during the second MESSENGER flyby of Mercury, when the IMF was southward, implied a cross-magnetosphere electric potential of ~30 kV or a mean dawn-to-dusk electric field of ~2 mV/m (*5*). This electric field implies a Dungey cycle time (i.e., time to drift in response to the dawn-to-dusk magnetospheric electric field from local noon to midnight in the polar cap, or from the northern boundary of the tail down to the cross-tail current sheet) at Mercury of ~2 min. The ~1-hour Dungey cycle time at Earth is believed to be the underlying reason for the ~1- to 3-hour duration of terrestrial substorms (*1*, *4*).

MESSENGER's third flyby of Mercury occurred on 29 September 2009. The IMF immediately preceding the flyby of Mercury had a variable north-south orientation and a magnitude of ~28 nT, ~50% stronger than for the previous encounters. Like the other MESSENGER flybys, the M3 trajectory was near equatorial, and the spacecraft entered the magnetosphere through the downstream dusk magnetosheath and exited just forward of the dawn terminator (Fig. 1). The inbound bow shock (BS) and (average) magnetopause (MP) crossing times were 20:56:06 and 21:27:45 UTC, respectively. The MESSENGER spacecraft autonomously terminated science observations and entered a "safe hold" at 21:48:37 UTC, so no outbound boundary crossings were measured. A fit to the MESSENGER and Mariner 10 averaged boundary crossings using methods and functional forms recently applied to Mercury (*6*–*9*) yielded mean subsolar bow shock and magnetopause planetocentric distances of 1.7 and

[1]Heliophysics Science Division, NASA Goddard Space Flight Center, Greenbelt, MD 20771, USA. [2]Johns Hopkins University Applied Physics Laboratory, Laurel, MD 20723, USA. [3]Laboratory for Atmospheric and Space Physics, University of Colorado, Boulder, CO 80303, USA. [4]Department of Physics and Astrophysical and Planetary Sciences Department, University of Colorado, Boulder, CO 80303, USA. [5]Solar System Exploration Division, NASA Goddard Space Flight Center, Greenbelt, MD 20771, USA. [6]Goddard Earth Science and Technology Center, University of Maryland, Baltimore County, Baltimore, MD 21228, USA. [7]Department of Astronomy, University of Maryland, College Park, MD 20742, USA. [8]Department of Atmospheric, Oceanic and Space Sciences, University of Michigan, Ann Arbor, MI 48109, USA. [9]Academy of Athens, Athens 11527, Greece. [10]Department of Terrestrial Magnetism, Carnegie Institution of Washington, Washington, DC 20015, USA. [11]Institute of Geophysics and Planetary Physics, University of California, Los Angeles, CA 90024, USA. [12]Department of Physics, Catholic University of America, Washington, DC 20064, USA. [13]Astronomical Institute, Academy of Sciences of the Czech Republic, Prague 14131, Czech Republic.

*To whom correspondence should be addressed. E-mail: james.a.slavin@nasa.gov